INTERNATIONAL JOURNAL FOR NUMERICAL METHODS IN FLUIDS
Int. J. Numer. Meth. Fluids 2001; **36**: 417–439 (DOI: 10.1002/fld.136)

Fourier analysis of several finite difference schemes for the one-dimensional unsteady convection–diffusion equation

J. M. C. Pereira and J. C. F. Pereira[1]*

Department of Mechanical Engineering/LASEF, Instituto Superior Técnico/Technical University of Lisbon, Lisbon, Portugal

SUMMARY

This paper reports a comparative study on the stability limits of nine finite difference schemes to discretize the one-dimensional unsteady convection–diffusion equation. The tested schemes are: (i) fourth-order compact; (ii) fifth-order upwind; (iii) fourth-order central differences; (iv) third-order upwind; (v) second-order central differences; and (vi) first-order upwind. These schemes were used together with Runge–Kutta temporal discretizations up to order six. The remaining schemes are the (vii) Adams–Bashforth central differences, (viii) the Quickest and (ix) the Leapfrog central differences. In addition, the dispersive and dissipative characteristics of the schemes were compared with the exact solution for the pure advection equation, or simple first or second derivatives, and numerical experiments confirm the Fourier analysis. The results show that fourth-order Runge–Kutta, together with central schemes, show good conditional stability limits and good dispersive and dissipative spectral resolution. Overall the fourth-order compact is the recommended scheme. Copyright © 2001 John Wiley & Sons, Ltd.

KEY WORDS: one-dimensional unsteady; convection–diffusion; Fourier analysis; stability limits

1. INTRODUCTION

Simulation of unsteady incompressible fluid flow phenomena is receiving increasing interest, either in the investigation of turbulent flow structure [direct numerical simulation (DNS) and large eddy simulation (LES)] or in the framework of engineering applications. Finite difference schemes have been used extensively in the simulations of those flows. Usually the criteria that set the maximum time step for explicit methods are the same criteria for time accuracy. That is, the time step is selected in order to resolve the characteristic time scales of interest, which very often favours the use of explicit schemes over the unconditionally stable implicit methods.

* Correspondence to: Department of Mechanical Engineering/LASEF, Instituto Superior Técnico/Technical University of Lisbon, Av. Rovisco Pais, 1049-001 Lisbon, Portugal. Tel.: +351 21 8417368; fax: +351 21 8495241.
[1] E-mail: jose@navier.ist.utl.pt

Received January 2000
Revised March 2000

For stable simulations of fluid flow by explicit finite difference schemes, the time step must be smaller than a critical time step. Since the pioneering work of Courant, Friedrichs and Levy (CFL; see Lax [1] for a historical perspective) the techniques for evaluating this time step are described in many textbooks, e.g. Roache [2] and Thomas [3]. Among them the Fourier method proposed by von Neumann or the matrix method, if boundary conditions should be also taken into account, are very popular and many studies have been reported investigating the stability limits of explicit finite difference analogues of the convection–diffusion equation, see, e.g. Rigal [4,5], Leonard [6], Clancy [7], Noye [8], Richardson and Ferrel [9] and Morton [10]. Theoretical studies involving generalization to multi-dimensional problems may be found in Hindmarsh *et al.* [11] and Rigal [12]. Other particular properties, such as conservation properties, non-linear instabilities, dissipation and dispersion, may be found in References [13–16] to mention but a few classical works.

The main objective of this paper is to report a comparative study of the stability limits of different convection discretization schemes in the framework of Runge–Kutta temporal discretization. We focus on the stability region for the one-dimensional unsteady convection–diffusion equation and dispersion and dissipation properties. The convection discretization schemes to be evaluated under Runge–Kutta of first-, second, fourth- and sixth-order are (i) fourth-order compact, see Lele [17]; (ii) fourth-order central differences; (iii) second-order central differences; (iv) fifth-order upwind, see Rai and Moin [18]; (v) third-order upwind; (vi) first-order upwind; and, in addition, the second-order accurate temporal discretization schemes: the (vii) Adams–Bashforth central differences; (viii) Leapfrog Duffort–Frankel; and (ix) Quickest [19]. Thus, several results in this work, in particular stability analysis of the one-dimensional transport equation are not new. However, the detailed comparison will provide complementary information for those interested in applications of Runge–Kutta multi-stage temporal discretization for practical fluid flow problems. Moreover, two families of discretization procedures involving symmetrical and unsymmetrical stencils for convection discretization are compared, including the high-order compact. The diffusion terms were always evaluated with symmetric finite difference stencils.

The results are presented mainly in a geometrical format for clarity and evaluated using MATHEMATICA to avoid algebraic errors. In addition, this tool allows us to easily manipulate complex expressions required to present the stability diagrams.

The different schemes for spatial and temporal discretization are presented in the next section. Section 3 presents the stability diagrams for the schemes tested and a spectral analysis of dispersion and dissipation errors. This is followed in Section 4 by numerical experiments with a periodic exponential-like function that demonstrates the conducted Fourier analysis. The paper ends with summary conclusions.

2. BRIEF DESCRIPTION OF THE NUMERICAL SCHEMES

In this section we will briefly outline the numerical discretization schemes under consideration.

The general differential equation to be studied is the convection–diffusion equation

$$\frac{\partial \phi}{\partial t} = -a\frac{\partial \phi}{\partial x} + v\frac{\partial^2 \phi}{\partial x^2} + f_\phi(x) \tag{2.1}$$

were ϕ is the scalar property to be transported, a is the field velocity and v is the diffusive coefficient. $f_\phi(x)$ is a force term that balances the external forces and, without the lack of generalization will not be considered in the following. In the next sections the discretization of the first and second derivatives of Equation (2.1) is presented for each scheme used.

2.1. Spatial discretization

2.1.1. First derivative. The general expression for the discrete approximation of the first derivative is

$$\left.\frac{\partial \phi}{\partial x}\right|_i \cong \frac{\alpha_{i-n}\phi_{i-n} + \cdots + \alpha_{i-1}\phi_{i-1} + \alpha_i\phi_i + \alpha_{i+1}\phi_{i+1} + \cdots + \alpha_{i+m}\phi_{i+m}}{\Delta x} \tag{2.2}$$

where α_i are coefficients to be defined and Δx, set to a constant, is the grid spacing. Controlling the m and n integer values and the α_i we can construct a lot of schemes with some formal truncation error order and/or some specific properties. For the non-symmetric schemes we suppose that a is positive, and so an upwind scheme will be characterized by $n > m$.

In the case of compact methods, an implicit relationship enforces the discrete value to depend on both the field variable and its own derivative

$$\left.\frac{\partial \phi}{\partial x}\right|_i \cong \phi'_i$$

so that

$$\beta_{i-p}\phi'_{i-p} + \cdots + \beta_i\phi'_i + \cdots + \beta_{i+q}\phi'_{i+q} = \frac{\alpha_{i-n}\phi_{i-n} + \cdots + \alpha_i\phi_i + \cdots + \alpha_{i+m}\phi_{i+m}}{\Delta x} \tag{2.3}$$

2.1.1.1. First-order upwind (Up1).

$$n = 1, \qquad m = 0$$

$$\alpha_{i-1} = -1, \qquad \alpha_i = 1$$

$$\varepsilon = \frac{1}{2}(\Delta x)^1$$

ε being the truncation error.

2.1.1.2. Third-order upwind (Up3).

$$n=2, \qquad m=1$$

$$\alpha_{i-2}=\frac{1}{6}, \qquad \alpha_{i-1}=-1, \qquad \alpha_i=\frac{1}{2}, \qquad \alpha_{i+1}=\frac{1}{3}$$

$$\varepsilon=\frac{1}{12}(\Delta x)^3$$

2.1.1.3. Fifth-order upwind (Up5).

$$n=3, \qquad m=2$$

$$\alpha_{i-3}=-\frac{1}{30}, \qquad \alpha_{i-2}=\frac{1}{4}, \qquad \alpha_{i-1}=-1, \qquad \alpha_i=\frac{1}{3}, \qquad \alpha_{i+1}=\frac{1}{2}$$

$$\alpha_{i+2}=-\frac{1}{20}$$

$$\varepsilon=\frac{1}{60}(\Delta x)^5$$

2.1.1.4. Second-order central (Cd2).

$$n=1, \qquad m=1$$

$$\alpha_{i-1}=-\frac{1}{2}, \qquad \alpha_i=0, \qquad \alpha_{i+1}=\frac{1}{2}$$

$$\varepsilon=\frac{1}{6}(\Delta x)^2$$

2.1.1.5. Fourth-order central (Cd4).

$$n=2, \qquad m=2$$

$$\alpha_{i-2}=\frac{1}{12}, \qquad \alpha_{i-1}=-\frac{2}{3}, \qquad \alpha_i=0, \qquad \alpha_{i+1}=\frac{2}{3}, \qquad \alpha_{i+2}=-\frac{1}{12}$$

$$\varepsilon=\frac{1}{30}(\Delta x)^4$$

2.1.1.6. Fourth-order central compact (CdC4).

$$n=1, \qquad m=1, \qquad p=1, \qquad q=1$$

$$\alpha_{i-1}=-\frac{3}{4}, \qquad \alpha_i=0, \qquad \alpha_{i+1}=\frac{3}{4}$$

$$\beta_{i-1}=\frac{1}{4}, \qquad \beta_i=1, \qquad \beta_{i+1}=\frac{1}{4}$$

$$\varepsilon=\frac{1}{120}(\Delta x)^4$$

2.1.2. Second derivative. The general expression for the discrete approximation of the second derivative is

$$\left.\frac{\partial^2\phi}{\partial x^2}\right|_i \cong \frac{\alpha_{i-n}\phi_{i-n}+\cdots+\alpha_{i-1}\phi_{i-1}+\alpha_i\phi_i+\alpha_{i+1}\phi_{i+1}+\cdots+\alpha_{i+m}\phi_{i+m}}{(\Delta x)^2} \tag{2.4}$$

where α_i are coefficients to be defined and Δx, set to a constant, is the grid spacing. Controlling the m and n integer values and the α_i we can construct a lot of schemes with some formal truncation error order and/or some specific properties.

In the case of compact methods, an implicit relationship enforces the discrete value to depend on both the field variable and its own derivative

$$\left.\frac{\partial^2\phi}{\partial x^2}\right|_i \cong \phi''_i$$

so that

$$\beta_{i-p}\phi''_{i-p}+\cdots+\beta_i\phi''_i+\cdots+\beta_{i+q}\phi''_{i+q}=\frac{\alpha_{i-n}\phi_{i-n}+\cdots+\alpha_i\phi_i+\cdots+\alpha_{i+m}\phi_{i+m}}{(\Delta x)^2} \tag{2.5}$$

2.1.2.1. Second-order central (Cd2).

$$n=1, \qquad m=1$$

$$\alpha_{i-1}=1, \qquad \alpha_i=-2, \qquad \alpha_{i+1}=1$$

$$\varepsilon=\frac{1}{12}(\Delta x)^2$$

2.1.2.2. Fourth-order central (Cd4).

$$n=2, \qquad m=2$$

$$\alpha_{i-2}=-\frac{1}{12}, \qquad \alpha_{i-1}=\frac{4}{3}, \qquad \alpha_i=-\frac{5}{2}, \qquad \alpha_{i+1}=\frac{4}{3}, \qquad \alpha_{i+2}=-\frac{1}{12}$$

$$\varepsilon=\frac{1}{90}(\Delta x)^4$$

2.1.2.3. Fourth-order central compact (CdC4).

$$n=1, \qquad m=1, \qquad p=1, \qquad q=1$$

$$\alpha_{i-1}=\frac{6}{5}, \qquad \alpha_i=-\frac{12}{5}, \qquad \alpha_{i+1}=\frac{6}{5}$$

$$\beta_{i-1}=\frac{1}{10}, \qquad \beta_i=1, \qquad \beta_{i+1}=\frac{1}{10}$$

$$\varepsilon=\frac{1}{200}(\Delta x)^4$$

2.2. Temporal discretization

The temporal discretization was performed by the standard Runge–Kutta schemes as well as by the well-known second-order Adams–Bashforth and Leapfrog and the third-order Quickest.

2.2.1. Runge–Kutta p-order (RKp). The standard up p-order Runge–Kutta schemes are defined as

$$\mathrm{RK}(p;\ z)=\sum_{i=0}^{p}\frac{z^i}{i!} \tag{2.6}$$

where z is an operator related to the spatial discretization. Each Runge–Kutta temporal discretization scheme can be written as

$$\phi^{n+1}=\mathrm{RK}(p;\ \Delta tf)\phi^n \tag{2.7}$$

where Δt is the time step and f is the spatial operator.

2.2.2. Adams–Bashforth second-order (AB2).

$$\phi^{n+1} = \phi^n + \frac{3}{2}\Delta t f(\phi^n) - \frac{1}{2}\Delta t f(\phi^{n-1}) \tag{2.8}$$

2.2.3. Leapfrog second-order (LF).

$$\phi^{n+1} = \phi^{n-1} + 2\Delta t f(\phi^n) \tag{2.9}$$

2.2.4. Quickest third-order (Q). The Quickest scheme may be presented as

$$\begin{aligned}
&\mathrm{grad}R = \phi^n_{i+1} - \phi^n_i \\
&\mathrm{grad}L = \phi^n_i - \phi^n_{i-1} \\
&\mathrm{curv}R = \phi^n_{i-1} - 2\phi^n_i + \phi^n_{i+1} \\
&\mathrm{curv}L = \phi^n_{i-2} - 2\phi^n_{i-1} + \phi^n_i \\
&\phi^{n+1}_i = \phi^n_i - c\left(\left(\frac{\phi^n_i + \phi^n_{i+1}}{2} - \frac{c}{2}\mathrm{grad}R - \frac{1}{6}(1 - c^2 - 3\gamma)\,\mathrm{curv}R\right)\right. \\
&\qquad \left. -\left(\frac{\phi^n_i + \phi^n_{i-1}}{2} - \frac{c}{2}\mathrm{grad}L - \frac{1}{6}(1 - c^2 - 3\gamma)\,\mathrm{curv}L\right)\right) \\
&\qquad +\gamma\left(\left(\mathrm{grad}R - \frac{c}{2}\mathrm{curv}R\right) - \left(\mathrm{grad}L - \frac{c}{2}\mathrm{curv}L\right)\right)
\end{aligned} \tag{2.10}$$

where $c = a\Delta t/\Delta x$ is the CFL number, commonly designated the Courant number and $\gamma = v\Delta t/\Delta x^2$ is the diffusive parameter.

Additional information related to this scheme may be found in Leonard [19], Durst *et al.* [20] or Pereira and Sousa [21].

3. FOURIER ANALYSIS

In this section we present the Fourier analysis of the schemes taking into account the stability limit by the von Neumann method and the spectral resolution as a function of the wavenumber.

3.1. Fourier analysis method

The Fourier analysis used here, see, e.g. Vichnevetsky and Bowles [22] and Hirsch [23], basically consists of applying a local Fourier series to the discretized equation by replacing each local ϕ by a corresponding Fourier mode

$$\phi_{i+q}^{n+p} = \Phi^p \, e^{Iq\beta\Delta x} = \Phi^p \, e^{Iq\theta} \tag{3.1}$$

where Φ^p is the amplitude at the pth time level, I is the imaginary number $\sqrt{-1}$ and θ is the cell wavenumber. Because of the linear behaviour of the Fourier series, a simple Fourier mode, which is *a priori* generic, is enough to be considered.

After proper algebraic manipulations, one obtains an expression for Φ or a polynomial of it. With the above notation the complex Φ represents the amplification factor which measures how the several Fourier modes in the field change with the time step as a function of Courant and the diffusive parameter. The condition $|\Phi| < 1$ for all wavenumbers θ, $\theta \in [0; \pi]$ is the guarantee of stability while its modulus and argument represents the evolution in amplitude and phase respectively.

3.2. Comparison of stability limits of different schemes

The stability limits of the Runge–Kutta temporal discretization (first-, second-, fourth- and sixth-order) combined with different schemes for convection and diffusion are shown Figure 1(a)–(f). The figures correspond to Up1Cd2, Up3Cd2, Up5Cd4, Cd2Cd2, Cd4Cd4 and CdC4CdC4 respectively (the first letters in the notation refer to the convective scheme). Each figure shows the stability limits as a function of Courant $c = a\Delta t/\Delta x$ and diffusive parameter $\gamma = v\Delta t/\Delta x^2$ for different Runge–Kutta temporal discretization schemes ranging from first-order to sixth-order of accuracy. As expected, the stability limit increases with the increase of Runge–Kutta stages. Convection discretization performed with upwind schemes show a similar trend characterized by a linearly decrease of Courant parameter, with an increase of the diffusive parameter up to a critical value. This behaviour is independent of the level of accuracy of the upwind scheme. However, the convection discretization schemes that use a symmetric stencil (central differences of compact central differences) show an opposite trend characterized by a maximum diffusive limit that occurs at a Courant number greater than zero. Also, the central differences show that the RK4 is stable for pure convection. The RK3, that is not shown, also displays a stable region for infinite Péclet number but the maximum Courant is approximately 0.6 of the displayed RK4 value.

Very often fluid flow calculations close to boundaries display a stability limit due to large diffusive parameters and low Courant numbers, which slightly favour upwind schemes. Fortunately, the use of non-symmetric stencils close to boundaries also displays a slightly larger stability limit in comparison with symmetric stencils. For a wide range of high Reynolds flows, the Courant numbers are larger far from boundaries than close to walls and the diffusive parameters follow an opposite trend. The RK4 displays the larger stability limit in terms of Courant parameter for low ($\lessapprox 0.05$) diffusive parameters and symmetric stencils. For upwind schemes, for convection the RK4 displays a Courant ≈ 1.7 at diffusive parameter equal to zero. The results displayed in Figure 1(a)–(f) add to the many published stability diagrams since Roache [2] for upwind or central schemes using first-order Euler temporal discretization. The same is true for the compact schemes after Lele [17].

Figure 1(g) shows the stability limits for the Leapfrog, Adams–Bashforth and Quickest schemes. The second-order Adams–Bashforth and the Leapforg temporal discretization schemes are used with central differences spatial discretization as is usual in the literature and

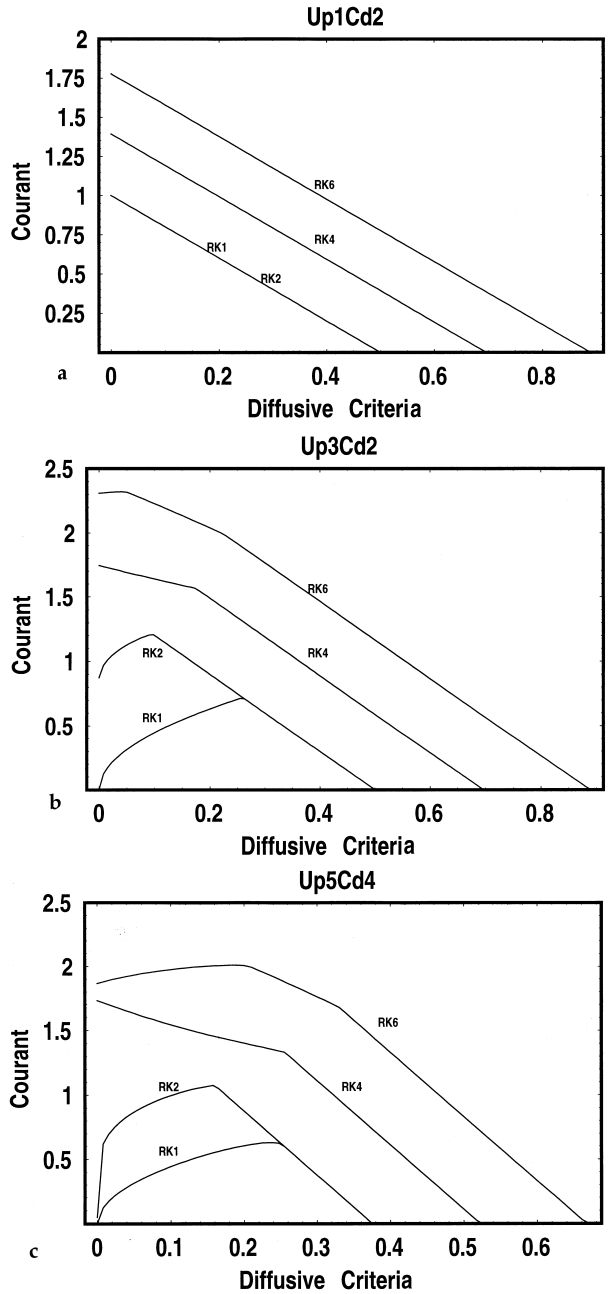

Figure 1. Stability limit for several temporal and spatial discretization schemes: (a) Runge–Kutta with Up1Cd2; (b) Runge–Kutta with Up3Cd2; (c) Runge–Kutta with Up5Cd4; (d) Runge–Kutta with Cd2cd2; (e) Runge–Kutta with Cd4Cd4; (f) Runge–Kutta with CdC4CdC4; (g) Stability limit for Q, LF and AB2.

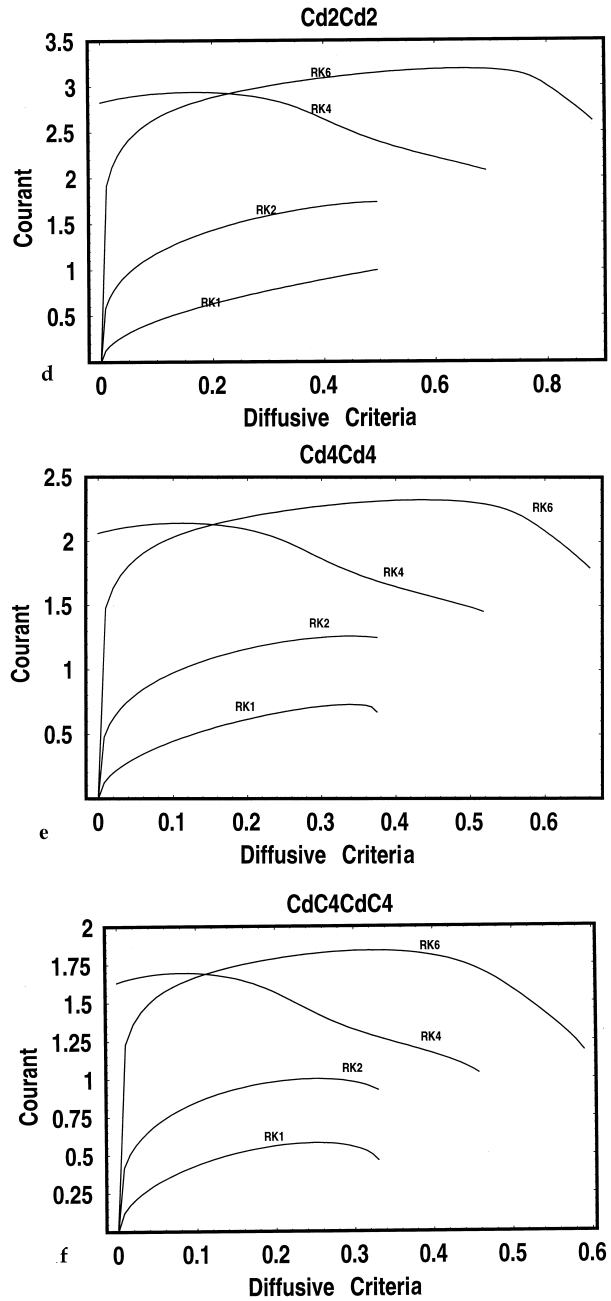

Figure 1 (*Continued*)

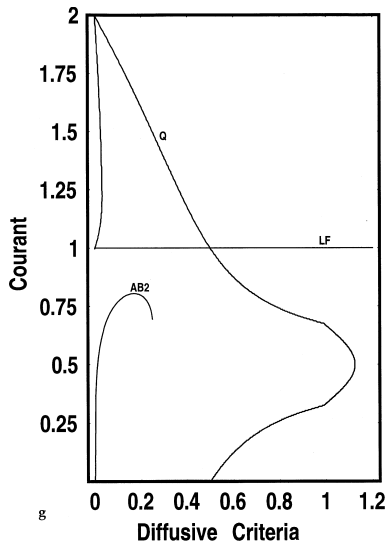

Figure 1 (*Continued*)

applications. The Adams–Bashforth scheme is unconditionally unstable for pure convection or for diffusive parameters greater than ≈ 0.25, see e.g. Ferziger [24]. For the convection–diffusion equation, it displays the maximum stability limit at a diffusive parameter approximately at 0.17, corresponding to a Courant number of about 0.8. The Leapfrog scheme, with the Duffort–Frankel as diffusive scheme, displays a stability limit corresponding to a Courant number ≤ 1 independently of the diffusive parameter, see e.g. Thomas [3]. The Quickest shows a stability diagram characterized by a high Courant number in the vicinity of a low diffusion parameter and afterwards a stability region in between two Courant numbers, see e.g. Leonard [6].

A comparison of the stability limits of all the tested schemes under RK1, RK2, RK4 or RK6 discretization is shown in Figure 2(a)–(d) respectively. If one does not consider the scheme's accuracy and only looks at the stability range for problems dictated with large diffusive parameter, the central differences are the best choice. Obviously they are especially appropriate for diffusion-dominated problems. If very high Péclet numbers (or very low diffusive parameters) are the main constraints of the problem, there is a clear option to use RK4 and symmetric stencils say compact high-order scheme.

Figure 3 shows the stability domain for several standard Runge–Kutta schemes plotted in the complex plane. The results show that for RK1 and RK2 the stability region of these methods is tangent to the imaginary axis by the left. For RK4 an improved stability is obtained when compared with the sixth-order method.

3.3. Spectral error analysis

In this section the dispersive and dissipative errors of each scheme are evaluated against the exact solution of a one-dimensional advection equation

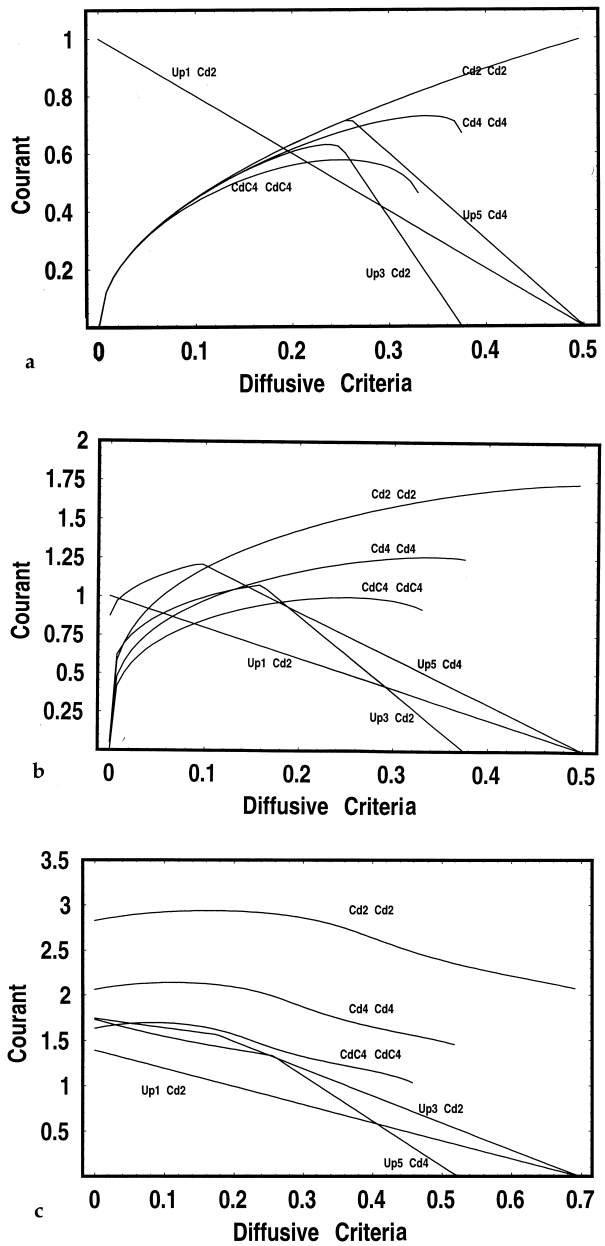

Figure 2. Stability for several spatial discretization schemes with: (a) RK1; (b) RK2; (c) RK4; (d) RK6.

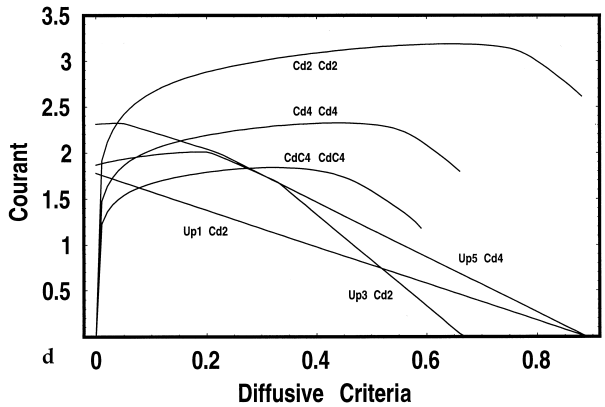

Figure 2 (*Continued*)

$$\frac{\partial \phi}{\partial t} = -a \frac{\partial \phi}{\partial x} \tag{3.2}$$

Using the exact solution

$$\phi(x, t) = \Phi \, e^{Iwt} \, e^{I\beta x} \tag{3.3}$$

the above advection equation is exactly satisfied for $w = -a\beta$, where w is the wave frequency and β is the wavenumber. So, the exponent of the first exponential term is imaginary and no dissipation exists. That is, the exact amplification factor is set equal to 1 and the exact

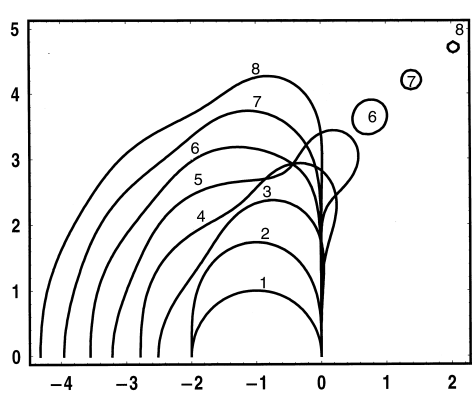

Figure 3. Stability domain for several standard RK schemes.

phase is $-c\theta$ (c being the Courant number) and $\theta = \beta \Delta x$, the frequency in terms of the several Fourier modes.

In addition to the knowledge of the finite difference scheme stability limit, one wishes to know the scheme characteristics with respect to dispersion and dissipation behaviour, see, e.g. Vichnevetsky and Bowles [22]. As is well known, the dispersion and dissipation of the scheme should be equal to those of the differential equation under consideration. This objective is also known not to be achieved, because the fluid flow equation(s) do not have general analytical solutions. Consequently, the scheme should have a good spectral resolution under simplified fluid flow models as a prerequisite to giving reliable solutions of the Navier–Stokes equations under practical meshes. In the case of meshes with a sufficient number of points per wave, it is well known that the spectral resolution of the scheme is proportional to its truncation error.

For steady fluid flow problems the schemes should follow the dispersive and dissipative behaviour of a first and second spatial derivatives. For this propose, Figure 4(a) and (b) show the spectral resolution for the first derivative using the procedure outlined by Lele [17] and Figure 4(c) and (d) display the results concerning the second derivative. The compact scheme shows the best spectral resolution for both derivatives.

Figure 5(a)–(c) shows the dissipative (or amplitude) error as a function of frequency (or wavenumber) for all the schemes under consideration, except for Adams–Bashforth, and for Courant numbers of 0.1, 0.5 and 1.0 respectively. The figures show that non-symmetric stencils, such as the first-, third- and fifth-order upwind schemes, may yield large amplitude errors and symmetric schemes (compact schemes and central difference, including Leapfrog) that do not display real parts in their spectrum show no dissipative errors, or at least very low ones. The analysis of Figure 5(a)–(c) also shows that by increasing the Courant number, the upwind schemes display increasing errors at higher frequencies. The analysis of the present problem revealed two special cases which are worth mentioning. The compact RK4 scheme displays at a Courant number of 1 a dissipative behaviour in between $\pi/2$ and $3\pi/4$ due to the evolution of the RK4 stability domain (Figure 3). The imaginary axis lies inside the stability domain while the central Runge–Kutta schemes display a stability limit that is tangent to the imaginary axis (Figure 3). The other special case is related to Quickest behaviour. The Quickest scheme shows increasing dissipative errors up to a Courant number equal to 0.5. Afterwards the scheme displays a decreasing amplitude error with wavenumber up to its stability limit of Courant number equal to 1. At this Courant number value the scheme does not show dissipation error. Another particular case is relative to the two solutions of the amplification factor of the Leapfrog scheme, which display zero dissipation error.

Figure 6(a)–(c) shows the dispersive error as a function of frequency for the tested schemes and for Courant numbers equal to 0.1, 0.5 and 1.0 respectively. The general trend is that all the schemes show dispersive (or phase) errors at high frequencies. The dispersive error increases with the Courant number with the exception of the particular behaviour of the Quickest scheme.

The dispersive error evolution of Runge–Kutta upwind p-order (p odd) is virtually equal to Runge–Kutta central schemes $(p+1)$ order, up to a Courant number equal to 0.5. The Quickest scheme also displays for the phase error a complex behaviour in the sense that dispersion errors are present with the exception of Courant numbers equal to 0.5 and 1.0. For

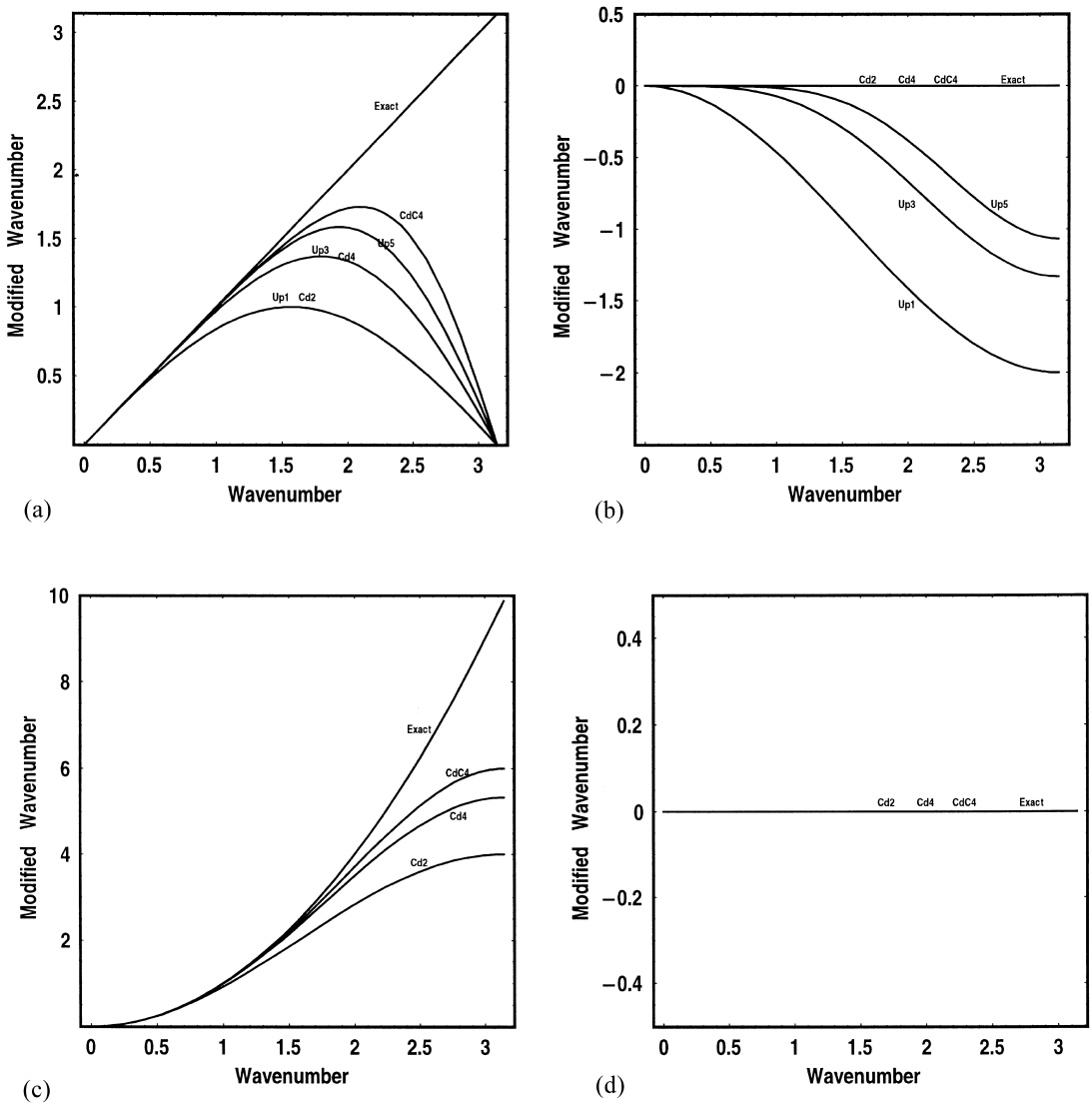

Figure 4. Spectral resolution for the (a) first derivative dispersion, (b) first derivative dissipation, (c) second derivative dispersion, (d) second derivative dissipation.

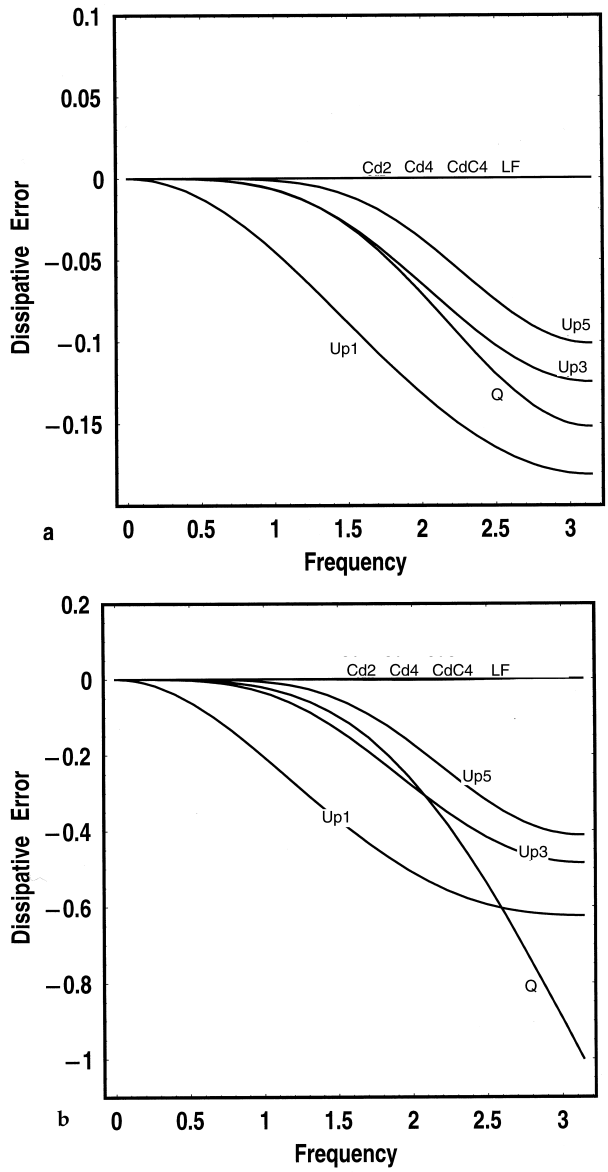

Figure 5. Dissipative error for several convective schemes: Courant = 0.1 (a); = 0.5 (b); = 1.0 (c).

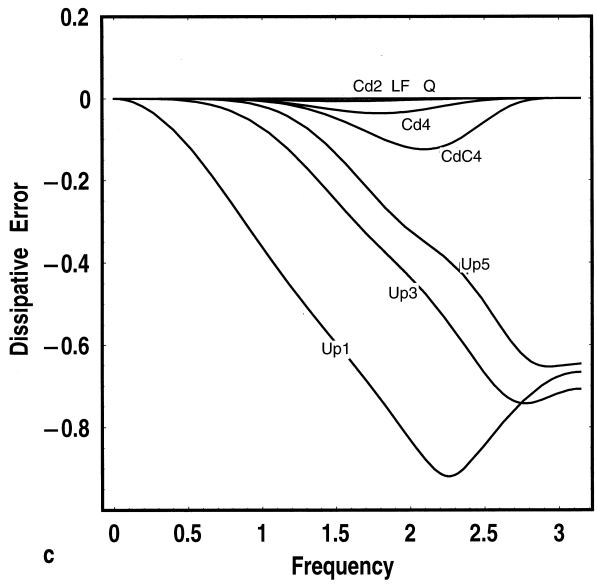

Figure 5 (*Continued*)

a Courant number equal to 1, Quickest displays the behaviour of a Lagrangian approximation, which is exact for the present one-dimensional problem and this is due to the inherent Leith-type of temporal approximation. Overall, the RK4 compact scheme shows the best resolution both in phase or in amplitude.

The Leapfrog scheme displays two solutions for the amplification factor, see e.g. Thomas [3]. One of them, not shown, displays very high dispersive errors for all frequency range but it is likely not present in the solution if the grid is not too coarse. The other solution shown in Figures 5 and 6 displays a dispersive error similar to central differences.

4. NUMERICAL EXPERIMENTS

Numerical experiments can be made either related to the stability diagrams or related to dissipation and dispersion errors. Numerical experiments to confirm the stability region have to be made with care because the von Neumann analysis does not take into consideration the boundary conditions. We have performed some tests to confirm the stable and unstable regions shown in Figures 1 and 2. However, they are not included in the figures for clarity.

Numerical experiments to confirm the dissipative or dispersive characteristics of the schemes for one-dimensional convection equation are presented in Figure 7, after two revolution periods of a C^{∞} exponential-like function

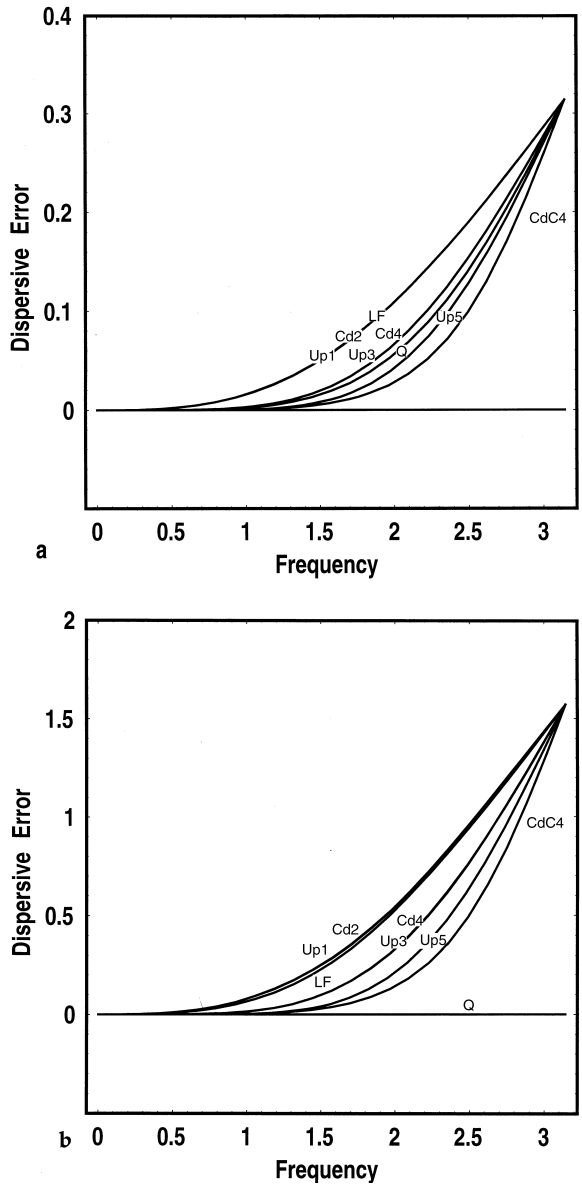

Figure 6. Dispersive error for several convective schemes: Courant = 0.1 (a); = 0.5 (b); = 1.0 (c).

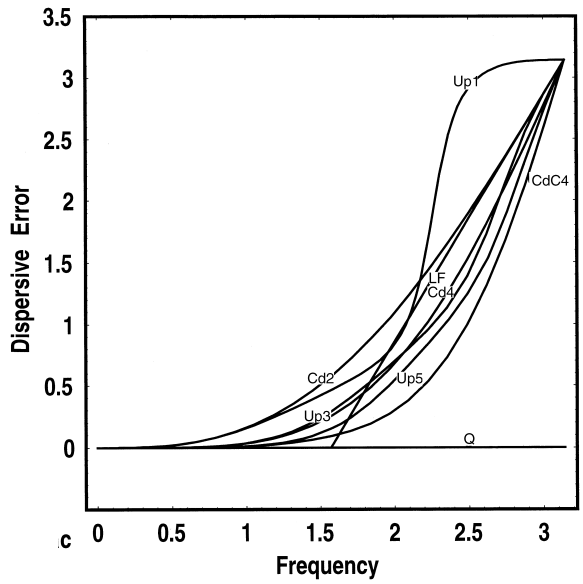

Figure 6 (*Continued*)

$$\phi = \begin{cases} \dfrac{e^{\left(\frac{-1}{(x-\frac{1}{4})(\frac{3}{4}-x)}\right)}}{e^{-16}} & \text{if } \dfrac{1}{4} < x < \dfrac{3}{4} \\ 0 & \text{elsewhere} \end{cases}$$

All results with the exception of Quickest are obtained with RK4 and the Courant number set equal to 0.5. A mesh with only 50 nodes was used to highlight the schemes solution differences.

Figure 7 shows the strong dissipation damping induced by the first-order accurate upwind scheme. The dissipation error decreases for third- and fifth-order upwind respectively. The compact scheme shows negligible dissipation (in fact there is no dissipation). These results agree very well with Figure 5(b). However, the results corresponding to RK4 and central differences (second- and fourth-order) suggest a dissipation error but their origin is related with an erroneous negative group velocity ($\mathscr{V}$).

Sinusoidal wave solutions interacting with the regular discretization of the domain of the equation produce a frequency dependent velocity. The theory of group velocity is important to explain the propagation of short wavelength spurious oscillations, which appear near discontinuities in discrete approximations of hyperbolic equations. Figure 8 shows the group velocity as a function of the wavenumber computed according to

$$\mathscr{V} = \frac{\mathrm{d}}{\mathrm{d}k}(k\hat{a})$$

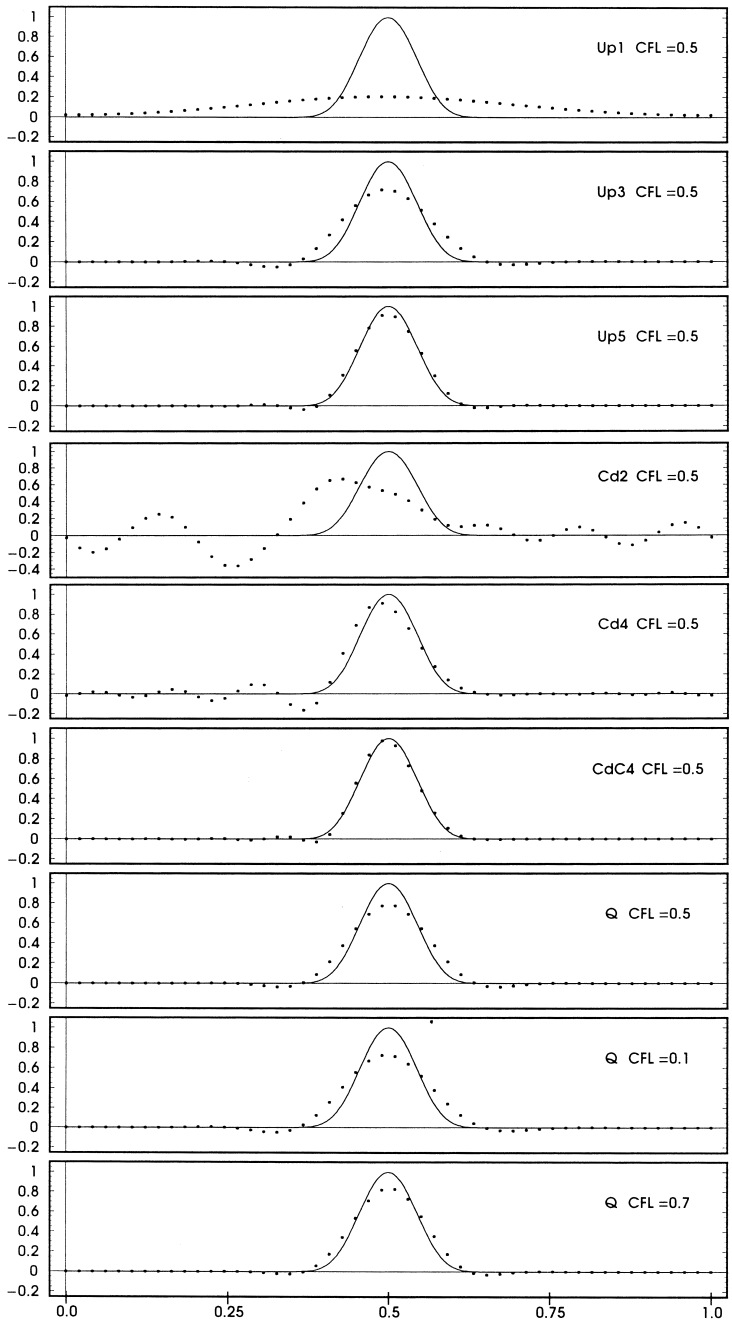

Figure 7. Numerical experiments with several convective schemes.

where k denotes the wavenumber and $\hat{a}$ the phase speed. The exact solution for a unit phase speed is $\mathscr{V} = 1.0$. Figure 8 shows that the group velocity deviates from unity with the increase in wavenumber. All the schemes display a region with negative group velocity for high wavenumbers while for low wavenumbers the deviation is inversely proportional to the scheme order of accuracy. The fourth-order compact scheme up to approximately $\frac{3}{4}\pi$ displays the best results, while the first- and third-order upwind schemes dissipate the spurious oscillations. The second- and fourth-order central schemes do not dissipate and the envelope of such spurious oscillations is observed to propagate at the group velocity rather than at the phase velocity. The second- and fourth-order central schemes display a non-negligible group velocity different from unity for very low wavenumbers. Consequently, the computational domain periodicity amplifies the differences between the phase and group velocities almost for all wavenumbers.

For the Quickest scheme, it shows an increasing dissipative error up to a Courant number equal to 0.5. Afterwards the scheme displays a decreasing amplitude error with wavenumber up to its stability limit of a Courant number equal to 1. Dispersion is seen to be zero at a Courant number equal to 0.5. Below this value, the common phase delay can be observed. For higher Courant number, in the case of 0.7, the phase velocity is greater than the correct one.

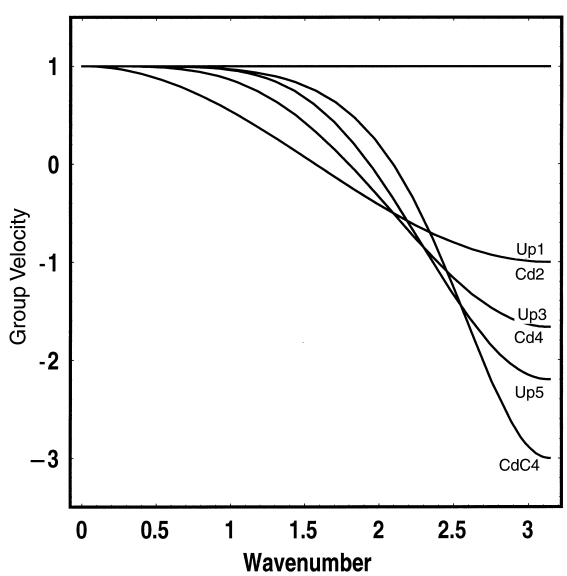

Figure 8. Group velocity for several convective schemes.

5. CONCLUSIONS

A Fourier analysis of different Runge–Kutta of first-, second-, fourth- and sixth-order was performed aiming to study the stability limits and phase and amplitude errors of different convection–diffusion discretization schemes applied to a one-dimensional transport equation. The global analysis showed that the standard RK4 displays a good stability region enhancing the stability limits of central difference schemes for convection discretization. Afterwards, a Fourier analysis of nine different schemes, including six RK4 schemes (compact fourth-order, central differences second- and fourth-order and upwind first-, third- and fifth-order) and two second-order accurate (Leapfrog and Adams–Bashforth) and the third-order Quickest was performed aiming to access their stability limit. In addition, the amplitude and phase errors were evaluated against the exact solution of a linear one-dimensional wave equation.

The main conclusions of the work can be summarized as follows:

(i) Among the standard Runge–Kutta schemes, the RK4 showed a good stability region and a better one compared with the RK6 if central differences are used in spatial discretization.
(ii) The first-order upwind scheme should not be used for any calculation of unsteady flows, even with RK4 temporal discretization.
(iii) Upwind schemes (third- and fifth-order) should be used with very low Courant numbers, otherwise dissipative errors may corrupt the solutions at high wavenumber (coarse grids).
(iv) The classical Adams–Bashforth and Leapfrog schemes are very good when second-order accuracy is only required.
(v) The Quickest (quadratic Leith-type of temporal discretization and third-order upstream spatial discretization) should be used together with very low Courant numbers otherwise too large dissipation errors are present.
(vi) Overall, the fourth-order compact/RK4 shows the best spectral resolution.
(vii) The reported stability diagram may be useful to the reader to establish the stability limit for one of the schemes as a prerequisite for general application if other relevant information concerning non-linear instability or stability in multidimensional space are not available for the selected method.

REFERENCES

1. Lax PD. Hyperbolic difference equations: a review of the Courant–Friedrichs–Levy paper in the light of recent developments. *IBM Journal* 1967; **March**: 235–238.
2. Roache PJ. *Computational Fluid Dynamics*. Hermosa: Albuquerque, NM, 1976.
3. Thomas JW. *Numerical Partial Differential Equations—Finite Difference Methods*. Springer: New York, 1995.
4. Rigal A. Numerical analysis of two-level finite difference schemes for unsteady diffusion–convection problems. *International Journal for Numerical Methods in Engineering* 1989; **28**: 1001–1021.
5. Rigal A. Numerical analysis of three-time-level finite difference schemes for unsteady diffusion–convection problems. *International Journal for Numerical Methods in Engineering* 1990; **30**: 307–330.
6. Leonard BP. Note on the von Neumann stability of the explicit FTCS convective diffusion equation. *Applied Mathematical Modeling* 1980; **4**: 401–403.

7. Clancy RM. A note on finite differencing of the advection–diffusion equation. *Monthly Weather Review* 1981; **109**: 1807–1809.
8. Noye BJ. Some three-level difference methods for simulating advection in fluids. *Computers and Fluids* 1991; **19**(1): 119–140.
9. Richardson JL, Ferrel RT. Unconditionally stable explicit algorithms for non-linear fluid dynamics problems. *Journal of Computational Physics* 1993; **104**: 69–74.
10. Morton KW. Stability of finite difference approximations to a diffusion–convection equation. *International Journal for Numerical Methods in Engineering* 1980; **15**: 677–683.
11. Hindmarsh AC, Gresho PM, Griffiths DF. The stability of explicit Euler time-integration for certain finite difference approximations of the multi-dimensional advection–diffusion equation. *International Journal for Numerical Methods in Fluids* 1984; **4**: 853–897.
12. Rigal A. Stability analysis of finite difference schemes for two-dimensional advection–diffusion problems. *International Journal for Numerical Methods in Fluids* 1991; **13**: 579–597.
13. Arakawa A. Computational design for long-term numerical integration of the equations of fluid motion: two-dimensional incompressible flow. Part I. *Journal of Computational Physics* 1966; **1**: 119–143.
14. Morton KW. Stability and convergence in fluid flow problems. *Proceedings of the Royal Society of London A* 1971; **323**: 237–253.
15. Roache PJ. On artificial viscosity. *Journal of Computational Physics* 1972; **10**: 169–184.
16. Warming RF, Hyett J. The modified equation approach to the stability and accuracy analysis of finite-difference methods. *Journal of Computational Physics* 1974; **14**: 159–179.
17. Lele SK. Compact finite difference schemes with spectral-like resolution. *Journal of Computational Physics* 1992; **103**: 16–42.
18. Rai MM, Moin P. Direct simulations of turbulent flow using finite-difference schemes. *Journal of Computational Physics* 1991; **96**: 15–53.
19. Leonard BP. A stable and accurate convective modeling procedure based on quadratic upstream interpolation. *Computer Method in Applied Mechanics and Engineering* 1979; **19**: 59–98.
20. Durst F, Pereira JCF, Tropea C. The plane symmetric sudden expansion flow at low Reynolds numbers. *Journal of Fluid Mechanics* 1993; **248**: 567–581.
21. Pereira JCF, Sousa JMM. Finite volume calculations of self-sustained oscillations in a grooved channel. *Journal of Computational Physics* 1993; **106**: 19–29.
22. Vichnevetsky R, Bowles JB. *Fourier Analysis of Numerical Approximations of Hyperbolic Equations*. SIAM: Philadelphia, PA, 1982.
23. Hirsch C. *Numerical Computation of Internal and External Flows. Fundamentals of Numerical Discretization*, vol. 1. Wiley: New York, 1988.
24. Ferziger JH. *Numerical Methods for Engineering Application*. Wiley: New York, 1982.

